Direct Power Control of Pulsewidth Modulated Rectifiers Without DC Voltage Oscillations Under Unbalanced Grid Conditions

Yongchang Zhang, *Senior Member, IEEE*, Jie Liu, Haitao Yang, *Student Member, IEEE*, and Jihao Gao

***Abstract*—Direct power control with space vector modulation (DPC-SVM) features simple structure, fast dynamic performance, and little tuning work. However, the conventional DPC-SVM cannot achieve accurate power control under unbalanced grid conditions. A modified DPC-SVM is thus proposed for accurate power control under both ideal and unbalanced grid conditions. Though the power control accuracy is improved when compared with the conventional DPC-SVM, it still suffers highly distorted grid current and dc voltage oscillations with an unbalanced network. Therefore, a power compensation method is subsequently derived aiming at the following targets: eliminating dc voltage oscillations, achieving sinusoidal grid current, and obtaining unity power factor. To that end, average grid-side reactive power and oscillations in converter-side active power are controlled as zero by simply adding a compensation to original power reference. Additionally, the proposed method does not require extraction of a positive sequence or negative sequence component of grid voltage. Compared with the conventional DPC-SVM in an ideal grid, only additional compensation of power reference is required. As a result, control performance can be significantly improved without substantial increase in complexity. The superiority of the proposed method over the prior DPC-SVM is validated by both simulation and experimental results obtained on a two-level pulsewidth modulation voltage source rectifier.**

***Index Terms*—Power compensation, predictive power control, unbalanced grid.**

Manuscript received August 10, 2017; revised October 27, 2017 and January 9, 2018; accepted February 2, 2018. Date of publication February 19, 2018; date of current version June 1, 2018.This work was supported in part by the National Natural Science Foundation of China under Grant 51577003 and Grant 61473002, and in part by Beijing Natural Science Foundation under Grant 3162012. *(Corresponding author: Haitao Yang.)*

Y. Zhang, J. Liu, and J. Gao are with the Inverter Technologies Engineering Research Center of Beijing, North China University of Technology, Beijing 100144, China, with the Collaborative Innovation Center of Electric Vehicles in Beijing, Beijing Institute of Technology, Beijing 100081, China, and also with the Collaborative Innovation Center of Key Power Energy-Saving Technologies in Beijing, North China University of Technology, Beijing 100144, China (e-mail: yozhang@ieee.org; 347090517@qq.com; gjhsky@163.com).

H. Yang is with the Inverter Technologies Engineering Research Center of Beijing, North China University of Technology, Beijing 100144, China, and also with the Faculty of Engineering and Information Technology, University of Technology Sydney, Ultimo, NSW 2007, Australia (e-mail: yhtseaky@gmail.com).

Color versions of one or more of the figures in this paper are available online at http://ieeexplore.ieee.org.

Digital Object Identifier 10.1109/TIE.2018.2807421

I. Introduction

OWING to the merits of bidirectional power flow, sinusoidal grid currents, and controllability of dc-link voltage, pulsewidth modulation (PWM) rectifiers are widely used in grid-tied renewable energy applications, such as wind turbine generation and solar power system [1]–[4]. In practical application, unbalanced grid voltages may occur due to poor stiffness of a weak grid, faults, unbalanced load, etc. As a consequence, control of PWM rectifiers should be designed to guarantee the proper operation under not only an ideal condition but also unbalanced grid conditions [3]–[5].

For the control of a PWM rectifier, the voltage-oriented control (VOC) is a popular strategy due to its simplicity and satisfactory steady-state performance. In VOC, two proportional-integral (PI) controllers are usually implemented in the synchronous reference frame for current regulation [6]. However, dynamic performance of a PI controller is usually limited due to the compromise among noise immunity, stability margin, and overshoot during transient process [7], [8]. Direct power control (DPC) was also widely investigated for a PWM rectifier [9]–[12]. Compared to VOC, the conventional table based DPC is much simpler and more robust against parameter variation with very fast dynamic performance. By further introducing space vector modulation (SVM) into DPC, better steady state performance can be obtained than that of table-based DPC [13]–[16]. Among various DPC methods with SVM, the one based on the concept of deadbeat control is preferable for its simple principle and easy implementation [13], [15].

In the design of most control schemes, three-phase grid voltages are assumed to be balanced. Conventional methods designed for ideal grid suffer from several shortcomings under unbalanced grid conditions, such as distorted grid currents and oscillations in the dc voltage [15], [17]. To solve these issues, many improved current control schemes and power control schemes have been developed. Current control schemes are better in producing lower current distortions, whereas power control schemes are superior in reducing power ripples. To improve the current waveform and enhance the rejection ability against voltage harmonics, grid voltages are fed forward to the main controller in [18] and [19] aiming at achieving balanced and sinusoidal grid currents. To avoid the phase detection of grid voltage and rotating transformation, current references for

achieving different control objectives are derived in stationary reference frame in [17]. Then, a proportional-resonant (PR) controller is adopted to achieve current regulation. In [20], the performance between PR controller and conventional PI controllers implemented in dual synchronous reference frame is compared. It is shown that the dynamic performance of conventional PI controllers is greatly influenced by the delay resulting from decomposition of a positive sequence component (PSC) and a negative sequence component (NSC). To enable the flexible selection of different control objectives (i.e., elimination of negative sequence current, elimination of active power ripples, and elimination of reactive power ripples), a generalized current reference is derived in [21] with the voltage sensorless operation.

Apart from the current control mentioned above, various power control methods are also investigated under an unbalanced grid condition. In [15], constant active power and sinusoidal grid currents are achieved by direct power control with space vector modulation (DPC-SVM) utilizing the extended power theory [22]. However, oscillations in dc-link voltage still exist. In [23], a compensation is added to the original power reference to eliminate the negative sequence current. The principle of power compensation in [23] can be extended to achieve other control targets, such as active power ripple elimination and reactive power ripple elimination, as shown in [24]. However, the sequence decomposition of grid voltage is required in the calculation of compensation. The relationship between employing the extended power theory and the power compensation is further evaluated in [25]. It is shown that two schemes are the same under specific circumstance. Unlike current control under unbalanced grid conditions, which has been comprehensively studied, power control schemes still need to be further investigated. For a PWM rectifier, one of the main control objectives is to obtain the constant dc voltage, even if under unbalanced grid conditions. So far, an existing power compensation method has not considered eliminating the ripple component in the dc voltage caused by an unbalanced network.

To satisfy the requirement of obtaining a ripple-free dc voltage, unity power factor, and sinusoidal grid currents, this paper proposes a power compensation method, which works well under both the balanced and unbalanced grid conditions. One contribution of this paper is that the proposed compensation scheme takes the elimination of the dc voltage ripple into account. Furthermore, the sequence decomposition of converter and grid voltages/currents is no longer required. After obtaining power reference, the conventional DPC-SVM is modified so that the actual power can accurately track its reference when grid voltages are unbalanced. Compared with DPC-SVM presented in [13], which can only work effectively under an ideal grid, the modified DPC-SVM further extend its application to an unbalanced grid condition. The merits of the whole control system include the following:

1) no ripple in dc-link voltage;
2) sinusoidal grid currents;
3) fast dynamic response;
4) no requirement of tuning work;
5) accurate power regulation under both ideal and unbalanced grid conditions.

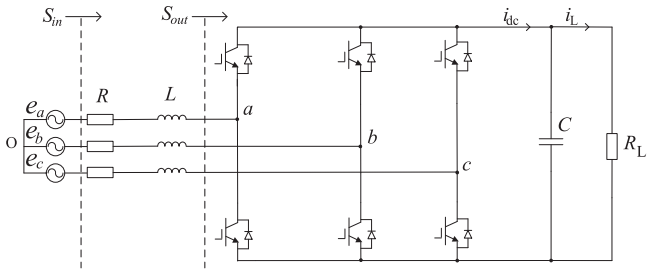

Fig. 1. Topology of a two-level PWM rectifier.

The effectiveness of the proposed DPC-SVM is confirmed by simulation and experimental results obtained on a two-level PWM rectifier.

The remaining part of this paper is organized as follows. Section II briefly introduces the model of a PWM rectifier under unbalanced grid conditions. In Section III, a modified DPC-SVM is proposed, which can achieve accurate power regulation under both ideal and unbalanced grid conditions. Additionally, a power compensation strategy is subsequently derived to obtain constant dc-link voltage and sinusoidal grid currents. Meanwhile, the average reactive power at grid side is kept zero. To verify the effectiveness of the proposed method, simulation and experimental results are elaborated and analyzed in Section IV. Finally, the conclusion is made in Section V.

II. Model of a PWM Rectifier Under an Unbalanced Network

A circuit diagram of a two-level PWM rectifier is shown in Fig. 1, where e_a, e_b, and e_c stand for three-phase grid voltages, and L and R are parameters of interconnecting reactor. The model of the two-level PWM rectifier can be expressed in the $\alpha\beta$ reference frame as

$$\boldsymbol{e}_{\alpha\beta} = R\boldsymbol{i}_{\alpha\beta} + L\frac{d\boldsymbol{i}_{\alpha\beta}}{dt} + \boldsymbol{v}_{\alpha\beta} \tag{1}$$

where $\boldsymbol{e}_{\alpha\beta} = e_\alpha + je_\beta$ stands for grid voltage vector, $\boldsymbol{i}_{\alpha\beta} = i_\alpha + ji_\beta$ is grid current vector, and $\boldsymbol{v}_{\alpha\beta} = v_\alpha + jv_\beta$ is the output voltage vector of the rectifier.

According to the instantaneous power theory [26], the grid-side complex power $\boldsymbol{S}_{\rm in}$ (ac side) and converter-side complex power $\boldsymbol{S}_{\rm out}$ (dc side) can be expressed as

$$\boldsymbol{S}_{\rm in} = P_{\rm in} + jQ_{\rm in} = 1.5\boldsymbol{i}^*_{\alpha\beta}\boldsymbol{e}_{\alpha\beta} \tag{2}$$

$$\boldsymbol{S}_{\rm out} = P_{\rm out} + jQ_{\rm out} = 1.5\boldsymbol{i}^*_{\alpha\beta}\boldsymbol{v}_{\alpha\beta} \tag{3}$$

where * indicates the conjugate of a complex vector.

The instantaneous input power $P_{\rm in}$ and $Q_{\rm in}$ under an unbalanced grid voltage can be expressed as [15], [24], [27]

$$\begin{cases} P_{\rm in} = \bar{P}_{\rm in} + \tilde{P}_{{\rm in},c}\cos(2\omega t) + \tilde{P}_{{\rm in},s}\sin(2\omega t) \\ Q_{\rm in} = \bar{Q}_{\rm in} + \tilde{Q}_{{\rm in},c}\cos(2\omega t) + \tilde{Q}_{{\rm in},s}\sin(2\omega t) \end{cases} \tag{4}$$

where

$$\begin{cases} \bar{P}_{\text{in}} = 1.5\left(\boldsymbol{i}_{dq}^{+}\odot\boldsymbol{e}_{dq}^{+}+\boldsymbol{i}_{dq}^{-}\odot\boldsymbol{e}_{dq}^{-}\right) \\ \bar{Q}_{\text{in}} = 1.5\left(\boldsymbol{i}_{dq}^{+}\otimes\boldsymbol{e}_{dq}^{+}+\boldsymbol{i}_{dq}^{-}\otimes\boldsymbol{e}_{dq}^{-}\right) \\ \tilde{P}_{\text{in},c} = 1.5\left(\boldsymbol{i}_{dq}^{+}\odot\boldsymbol{e}_{dq}^{-}+\boldsymbol{i}_{dq}^{-}\odot\boldsymbol{e}_{dq}^{+}\right) \\ \tilde{Q}_{\text{in},c} = 1.5\left(\boldsymbol{i}_{dq}^{+}\otimes\boldsymbol{e}_{dq}^{-}+\boldsymbol{i}_{dq}^{-}\otimes\boldsymbol{e}_{dq}^{+}\right) \\ \tilde{P}_{\text{in},s} = 1.5\left(\boldsymbol{i}_{dq}^{+}\otimes\boldsymbol{e}_{dq}^{-}-\boldsymbol{i}_{dq}^{-}\otimes\boldsymbol{e}_{dq}^{+}\right) \\ \tilde{Q}_{\text{in},s} = 1.5\left(\boldsymbol{i}_{dq}^{-}\odot\boldsymbol{e}_{dq}^{+}-\boldsymbol{i}_{dq}^{+}\odot\boldsymbol{e}_{dq}^{-}\right) \end{cases} \tag{5}$$

$\boldsymbol{e}_{dq}^{+}=e_d^{+}+\text{j}e_q^{+}$ and $\boldsymbol{i}_{dq}^{+}=i_d^{+}+\text{j}i_q^{+}$ denote the PSC of the grid voltage and grid current in the positive sequence synchronous reference frame; $\boldsymbol{e}_{dq}^{-}=e_d^{-}+je_q^{-}$ and $\boldsymbol{i}_{dq}^{-}=i_d^{-}+ji_q^{-}$ represent the NSC of the grid voltage and grid current in the negative sequence synchronous reference frame; the superscripts "+" and "−" represent PSC and NSC of a vector, respectively; the subscripts "c" and "s" denote cosine and sine components of power ripples, respectively; the hat "¯" and "˜" denote the dc component and ripple component of the power, respectively; $\odot$ and $\otimes$ represent the dot product and cross product of two complex vectors, respectively.

Similarly, the instantaneous output power P_{out} and Q_{out} as shown in (3) can be expressed as

$$\begin{cases} P_{\text{out}} = \bar{P}_{\text{out}}+\tilde{P}_{\text{out},c}\cos(2\omega t)+\tilde{P}_{\text{out},s}\sin(2\omega t) \\ Q_{\text{out}} = \bar{Q}_{\text{out}}+\tilde{Q}_{\text{out},c}\cos(2\omega t)+\tilde{Q}_{\text{out},s}\sin(2\omega t) \end{cases} \tag{6}$$

where

$$\begin{cases} \bar{P}_{\text{out}} = 1.5\left(\boldsymbol{i}_{dq}^{+}\odot\boldsymbol{v}_{dq}^{+}+\boldsymbol{i}_{dq}^{-}\odot\boldsymbol{v}_{dq}^{-}\right) \\ \bar{Q}_{\text{out}} = 1.5\left(\boldsymbol{i}_{dq}^{+}\otimes\boldsymbol{v}_{dq}^{+}+\boldsymbol{i}_{dq}^{-}\otimes\boldsymbol{v}_{dq}^{-}\right) \\ \tilde{P}_{\text{out},c} = 1.5\left(\boldsymbol{i}_{dq}^{+}\odot\boldsymbol{v}_{dq}^{-}+\boldsymbol{i}_{dq}^{-}\odot\boldsymbol{v}_{dq}^{+}\right) \\ \tilde{Q}_{\text{out},c} = 1.5\left(\boldsymbol{i}_{dq}^{+}\otimes\boldsymbol{v}_{dq}^{-}+\boldsymbol{i}_{dq}^{-}\otimes\boldsymbol{v}_{dq}^{+}\right) \\ \tilde{P}_{\text{out},s} = 1.5\left(\boldsymbol{i}_{dq}^{+}\otimes\boldsymbol{v}_{dq}^{-}-\boldsymbol{i}_{dq}^{-}\otimes\boldsymbol{v}_{dq}^{+}\right) \\ \tilde{Q}_{\text{out},s} = 1.5\left(\boldsymbol{i}_{dq}^{-}\odot\boldsymbol{v}_{dq}^{+}-\boldsymbol{i}_{dq}^{+}\odot\boldsymbol{v}_{dq}^{-}\right) \end{cases} \tag{7}$$

It can be found from (4)–(7) that the PSC and NSC of the grid voltage and grid current are required. To simplify the calculation process, original vector and its delayed value will be used in the following derivation. According to [28] and [29], we can obtain PSC and NSC of $\boldsymbol{e}_{\alpha\beta}$, $\boldsymbol{v}_{\alpha\beta}$, and $\boldsymbol{i}_{\alpha\beta}$ as

$$\begin{bmatrix} \boldsymbol{e}_{dq}^{+} \\ \boldsymbol{e}_{dq}^{-} \end{bmatrix} = \frac{1}{2}\begin{bmatrix} e^{-j\omega t} & je^{-j\omega t} \\ e^{j\omega t} & -je^{j\omega t} \end{bmatrix}\begin{bmatrix} \boldsymbol{e}_{\alpha\beta} \\ \boldsymbol{e}_{\alpha\beta}^{'} \end{bmatrix} \tag{8}$$

$$\begin{bmatrix} \boldsymbol{v}_{dq}^{+} \\ \boldsymbol{v}_{dq}^{-} \end{bmatrix} = \frac{1}{2}\begin{bmatrix} e^{-j\omega t} & je^{-j\omega t} \\ e^{j\omega t} & -je^{j\omega t} \end{bmatrix}\begin{bmatrix} \boldsymbol{v}_{\alpha\beta} \\ \boldsymbol{v}_{\alpha\beta}^{'} \end{bmatrix} \tag{9}$$

$$\begin{bmatrix} \boldsymbol{i}_{dq}^{+} \\ \boldsymbol{i}_{dq}^{-} \end{bmatrix} = \frac{1}{2}\begin{bmatrix} e^{-j\omega t} & je^{-j\omega t} \\ e^{j\omega t} & -je^{j\omega t} \end{bmatrix}\begin{bmatrix} \boldsymbol{i}_{\alpha\beta} \\ \boldsymbol{i}_{\alpha\beta}^{'} \end{bmatrix} \tag{10}$$

where $\boldsymbol{e}_{\alpha\beta}^{'}$, $\boldsymbol{v}_{\alpha\beta}^{'}$, and $\boldsymbol{i}_{\alpha\beta}^{'}$ denote their quadrature values that lag $\boldsymbol{e}_{\alpha\beta}$, $\boldsymbol{v}_{\alpha\beta}$, and $\boldsymbol{i}_{\alpha\beta}$ by 90 electrical degrees, respectively.

Substituting (8)–(10) into (5) and (7), the dc component of the input power and the gains of ripple component of the output power can be obtained as

$$\begin{cases} \bar{P}_{\text{in}} = \frac{3}{4}(\boldsymbol{i}_{\alpha\beta}\odot\boldsymbol{e}_{\alpha\beta}+\boldsymbol{i}_{\alpha\beta}^{'}\odot\boldsymbol{e}_{\alpha\beta}^{'}) \\ \bar{Q}_{\text{in}} = \frac{3}{4}(\boldsymbol{i}_{\alpha\beta}\otimes\boldsymbol{e}_{\alpha\beta}+\boldsymbol{i}_{\alpha\beta}^{'}\otimes\boldsymbol{e}_{\alpha\beta}^{'}) \end{cases} \tag{11}$$

$$\begin{cases} \tilde{P}_{\text{out},c} = \frac{3}{4}\left(k_1\cos(2\omega t)+k_2\sin(2\omega t)\right) \\ \tilde{P}_{\text{out},s} = \frac{3}{4}\left(-k_2\cos(2\omega t)+k_1\sin(2\omega t)\right) \end{cases} \tag{12}$$

where

$$\begin{cases} k_1 = \boldsymbol{i}_{\alpha\beta}\odot\boldsymbol{v}_{\alpha\beta}-\boldsymbol{i}_{\alpha\beta}^{'}\odot\boldsymbol{v}_{\alpha\beta}^{'} \\ k_2 = \boldsymbol{i}_{\alpha\beta}\odot\boldsymbol{v}_{\alpha\beta}^{'}+\boldsymbol{i}_{\alpha\beta}^{'}\odot\boldsymbol{v}_{\alpha\beta} \end{cases}. \tag{13}$$

III. DPC-SVM With the Elimination of DC Voltage Oscillations

A. DPC-SVM Under Unbalanced Grid Conditions

Since

$$\boldsymbol{e}_{\alpha\beta}=\boldsymbol{e}_{\alpha\beta}^{+}+\boldsymbol{e}_{\alpha\beta}^{-}. \tag{14}$$

The derivative of the grid voltage can be solved as

$$\begin{aligned} \frac{d\boldsymbol{e}_{\alpha\beta}}{dt} &= j\omega\boldsymbol{e}_{\alpha\beta}^{+}-j\omega\boldsymbol{e}_{\alpha\beta}^{-}=-\omega\left(-j\boldsymbol{e}_{\alpha\beta}^{+}+j\boldsymbol{e}_{\alpha\beta}^{-}\right) \\ &= -\omega\boldsymbol{e}_{\alpha\beta}^{'}. \end{aligned} \tag{15}$$

Similarly, the derivative of $\boldsymbol{e}_{\alpha\beta}^{'}$ can be obtained as

$$\frac{d\boldsymbol{e}_{\alpha\beta}^{'}}{dt}=\omega\boldsymbol{e}_{\alpha\beta}. \tag{16}$$

According to (1), (2), and (15), the derivative of grid-side complex power can be deduced as

$$\frac{d\boldsymbol{S}_{\text{in}}}{dt}=\frac{1}{L}\left[\frac{3}{2}\left(|\boldsymbol{e}|^2-\boldsymbol{v}^{*}\boldsymbol{e}\right)-(R+J\omega L)\boldsymbol{S}_{\text{in}}\right] \tag{17}$$

where

$$J=\frac{\boldsymbol{e}_{\alpha\beta}^{'}}{\boldsymbol{e}_{\alpha\beta}}. \tag{18}$$

Applying first-order Euler discretization to (17), the following equation can be obtained:

$$\boldsymbol{S}_{\text{in}}^{k+1}=\boldsymbol{S}_{\text{in}}^{k}+\frac{T_s}{L}\left[\frac{3}{2}(|\boldsymbol{e}^{k}|^2-(\boldsymbol{v}^{k})^{*}\boldsymbol{e}^{k})-(R+J\omega L)\boldsymbol{S}_{\text{in}}^{k}\right] \tag{19}$$

where T_s is the control period. For deadbeat power control, actual power should be equal to the reference at the next sampling instant, i.e.,

$$\boldsymbol{S}_{\text{in}}^{k+1}=\boldsymbol{S}^{\text{ref}}. \tag{20}$$

Solving (20) based on (19), the desired voltage vector nullifying the tracking error of complex power in the next control period is obtained as

$$\boldsymbol{v}^{\text{ref}}=\boldsymbol{e}^{k}-\frac{2}{3}\left(\frac{(R+J^{k}\omega L)\boldsymbol{S}_{\text{in}}^{k}}{\boldsymbol{e}^{k}}\right)^{*}-\frac{2L}{3T_s}\left(\frac{\boldsymbol{S}^{\text{ref}}-\boldsymbol{S}_{\text{in}}^{k}}{\boldsymbol{e}^{k}}\right)^{*}. \tag{21}$$

For an ideal grid, $J = \boldsymbol{e}'_{\alpha\beta}/\boldsymbol{e}_{\alpha\beta} = -j$ holds. In this case, $\boldsymbol{v}^{\mathrm{ref}}$ in (21) is the same as that of the conventional DPC-SVM presented in [15], which is a special case of (21) in this paper. It will be shown in Section IV that the conventional DPC-SVM cannot achieve accurate power regulation with unbalanced grid voltages, whereas the modified DPC-SVM in this paper can work properly under both ideal and unbalanced grid conditions.

B. Reference Compensation for Eliminating DC Voltage Ripples

Although the DPC-SVM in Section III-A can achieve accurate power tracking with unbalanced grid voltages, it suffers from highly distorted current and oscillations in the dc-link voltage if power references are kept the same as that derived under the ideal grid voltage. In this paper, a power compensation scheme will be proposed to obtain sinusoidal grid current and unity power factor while eliminating the oscillation in dc-link voltage under an unbalanced network. As the dc voltage oscillation is related to the active power ripple in the converter side, the control targets can be mathematically expressed based on (11) and (12) as follows:

$$\begin{cases} \bar{P}_{\mathrm{in}} = \frac{3}{4}(\boldsymbol{i}_{\alpha\beta} \odot \boldsymbol{e}_{\alpha\beta} + \boldsymbol{i}'_{\alpha\beta} \odot \boldsymbol{e}'_{\alpha\beta}) = P^{\mathrm{ref}} \\ \bar{Q}_{\mathrm{in}} = \frac{3}{4}(\boldsymbol{i}_{\alpha\beta} \otimes \boldsymbol{e}_{\alpha\beta} + \boldsymbol{i}'_{\alpha\beta} \otimes \boldsymbol{e}'_{\alpha\beta}) = 0 \\ \tilde{P}_{\mathrm{out},c} = \frac{3}{4}(k_1 \cos(2\omega t) + k_2 \sin(2\omega t)) = 0 \\ \tilde{P}_{\mathrm{out},s} = \frac{3}{4}(-k_2 \cos(2\omega t) + k_1 \sin(2\omega t)) = 0 \end{cases}. \tag{22}$$

From (13) and (22), the final current reference vector can be calculated as

$$\begin{aligned} \begin{bmatrix} i_\alpha^{\mathrm{ref}} \\ i_\beta^{\mathrm{ref}} \end{bmatrix} &= \frac{4P^{\mathrm{ref}}}{3\triangle} \begin{bmatrix} (v_\alpha v'_\beta - v_\beta v'_\alpha)e_\alpha \\ (v_\alpha v'_\beta - v_\beta v'_\alpha)e_\beta \end{bmatrix} \\ &+ \frac{4P^{\mathrm{ref}}}{3\triangle} \begin{bmatrix} (v_\alpha v_\beta + v'_\beta v'_\alpha)e'_\alpha \\ -(v_\alpha v_\beta + v'_\beta v'_\alpha)e'_\beta \end{bmatrix} \\ &+ \frac{4P^{\mathrm{ref}}}{3\triangle} \begin{bmatrix} (v_\beta^2 + v_\beta'^2)e'_\beta \\ -(v_\alpha^2 + v_\alpha'^2)e'_\alpha \end{bmatrix} \end{aligned} \tag{23}$$

where $\triangle = (v_\alpha v'_\beta - v_\beta v'_\alpha)(e_\alpha^2 + e_\alpha'^2 + e_\beta^2 + e_\beta'^2) + (e_\alpha e'_\beta - e'_\alpha e_\beta)(v_\alpha^2 + v_\alpha'^2 + v_\beta^2 + v_\beta'^2)$. The new complex power reference can then be calculated from the current reference as

$$\boldsymbol{S}_{\mathrm{new}}^{\mathrm{ref}} = 1.5\boldsymbol{i}^{\mathrm{ref}*}\boldsymbol{e} \tag{24}$$

where $\boldsymbol{i}^{\mathrm{ref}} = i_\alpha^{\mathrm{ref}} + j i_\beta^{\mathrm{ref}}$.

As the original power reference $\boldsymbol{S}^{\mathrm{ref}}$ is known, a more straightforward and natural solution is to add an appropriate compensation term to the original power reference. The power compensation value $\boldsymbol{S}^{\mathrm{comp}}$ is calculated as $\boldsymbol{S}^{\mathrm{comp}} = \boldsymbol{S}_{\mathrm{new}}^{\mathrm{ref}} - \boldsymbol{S}^{\mathrm{ref}}$ and its components can be expressed as follows:

$$\begin{aligned} P^{\mathrm{comp}} = \frac{P^{\mathrm{ref}}}{\triangle} \Big[&(e_\alpha^2 + e_\beta^2 - e_\alpha'^2 - e_\beta'^2)(v_\alpha v'_\beta - v_\beta v'_\alpha) \\ &- (v_\alpha^2 + v_\alpha'^2 - v_\beta^2 - v_\beta'^2)(e_\alpha e'_\beta + e_\beta e'_\alpha) \\ &+ 2(e_\alpha e'_\alpha - e_\beta e'_\beta)(v_\alpha v_\beta + v'_\alpha v'_\beta) \Big] \end{aligned} \tag{25}$$

$$\begin{aligned} Q^{\mathrm{comp}} = \frac{P^{\mathrm{ref}}}{\triangle} \Big[&2e_\alpha e'_\alpha(v_\alpha^2 + v_\alpha'^2) + 2e_\beta e'_\beta(v_\beta^2 + v_\beta'^2) \\ &+ 2(e_\alpha e'_\beta + e_\beta e'_\alpha)(v_\alpha v_\beta + v'_\alpha v'_\beta) \Big]. \end{aligned} \tag{26}$$

The control diagram of the proposed DPC-SVM with power compensation is shown in Fig. 2. Compared with the structure of the conventional DPC-SVM under ideal grid conditions, there is only an additional power compensation block. After obtaining the power compensation according to (25) and (26), the reference voltage $\boldsymbol{v}^{\mathrm{ref}}$ that can force actual power to follow their references is calculated according to (21). Finally, the SVM is used to generate switching signals for the converter to synthesize the calculated $\boldsymbol{v}^{\mathrm{ref}}$.

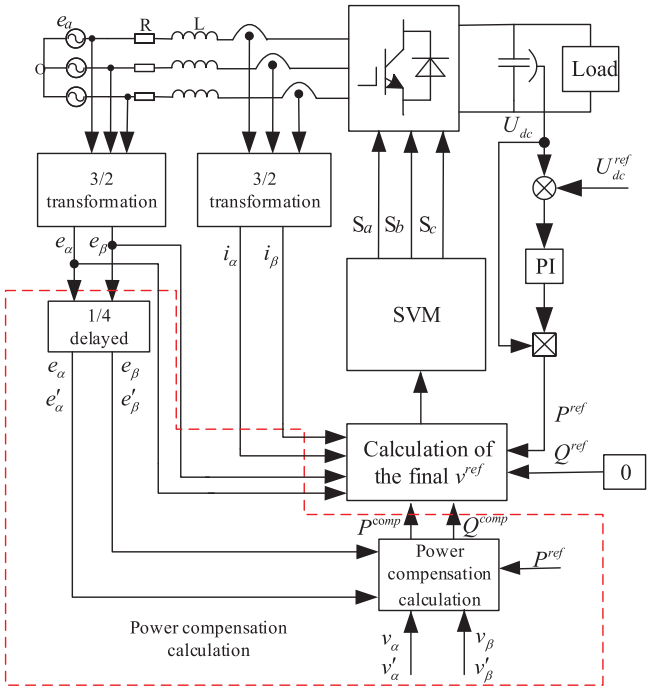

Fig. 2. Control diagram of the proposed DPC-SVM.

C. Design of a DC Voltage Controller

The dynamics of the dc voltage can be described as

$$C\frac{dU_{\mathrm{dc}}}{dt} = i_{\mathrm{dc}} - i_L \tag{27}$$

where C denotes the dc-link capacitor; i_{dc} represents the rectifier-side dc current as shown in Fig. 1, and i_L is the load current. Neglecting power losses, the dc-side output power should

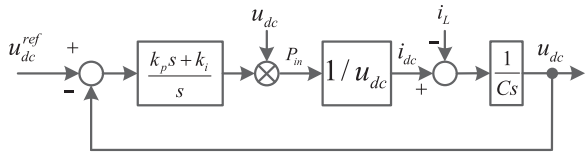

Fig. 3. Control diagram of the dc voltage regulation loop.

TABLE I
SYSTEM AND CONTROL PARAMETERS

System parameters	Symbol	Value
Line resistance	R	0.3 Ω
Line inductance	L	10 mH
Line–line voltage	U_N	150 V
Line voltage frequency	f_g	50 Hz
Load resistance	R_L	100 Ω
Sampling period	T_s	100 μs

be equal to the ac-side input power, i.e.,

$$P_{\rm in} = U_{\rm dc} i_{\rm dc}. \tag{28}$$

Based on (27) and (28), the following equation can be derived:

$$C\frac{dU_{\rm dc}}{dt} = \frac{P_{\rm in}}{U_{\rm dc}} - i_L. \tag{29}$$

From the above-mentioned equations, the control diagram of the dc voltage regulation loop can be depicted in Fig. 3. It should be noted that the PI output is multiplied by $U_{\rm dc}$ to cancel the gain $1/U_{\rm dc}$ in (29). In this way, PI gains can be tuned independent of $U_{\rm dc}$. The transfer function can be easily derived as

$$\frac{U_{\rm dc}}{U_{\rm dc}^{\rm ref}} = \frac{2\xi\omega_n s + \omega_n^2}{s^2 + 2\xi\omega_n s + \omega_n^2} \tag{30}$$

where $\xi = k_p/(2\sqrt{k_i C})$ and $\omega_n = \sqrt{k_i/C}$; k_p and k_i are PI gains, which need to be designed, that can be solved as

$$k_p = 2C\xi\omega_n \tag{31}$$

$$k_i = C\omega_n^2. \tag{32}$$

It is seen from (30) that the dc voltage regulation loop is a second-order system. In this paper, the damping ratio ξ is set as $\xi = \sqrt{2}/2$, which is usually selected for acceptable overshoot during transient process. And ω_n is chosen as $\omega_n = 100$ rad/s for the compromise between dynamic responses and immunity against noises and harmonics. Experimental results shown in Section IV-B can confirm the effectiveness of the selected PI gains.

IV. Simulation and Experimental Results

A. Simulation Results

To verify the effectiveness of the proposed method, it is tested in the environment of MATLAB/Simulink. The sampling frequency is set as 10 kHz for all the methods presented in this paper. Other control and system parameters are shown in Table I. First, the validity of the modified DPC-SVM (MDPC-SVM) in Section III-A is tested and compared with the conventional

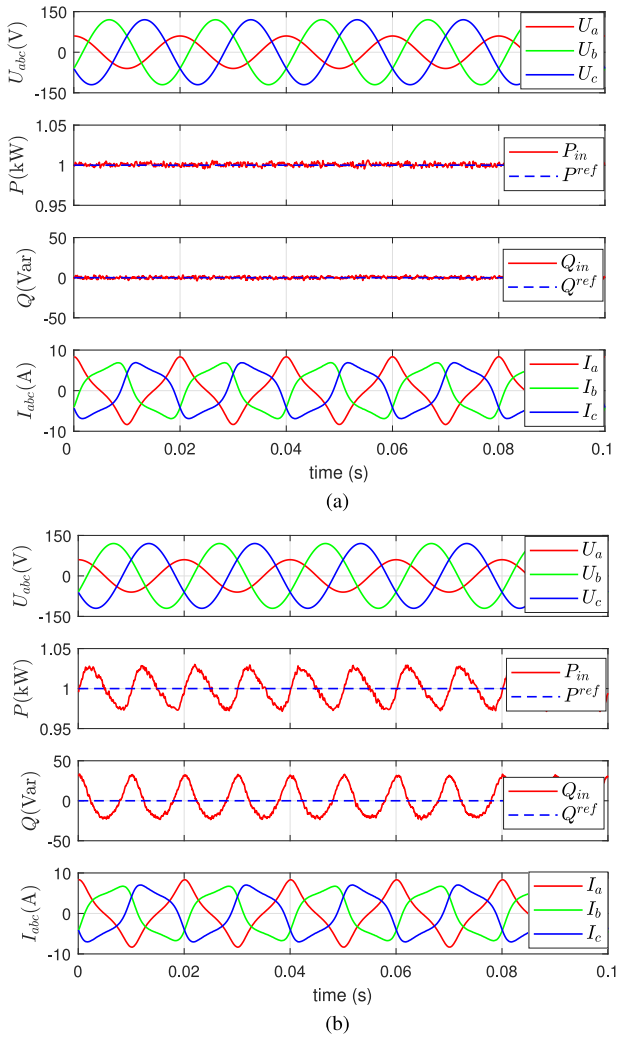

Fig. 4. Simulation results of U_{abc}, $P_{\rm in}$, $P^{\rm ref}$, $Q_{\rm in}$, $Q^{\rm ref}$, and I_{abc} for (a) MDPC-SVM and (b) CDPC-SVM.

DPC-SVM (CDPC-SVM) introduced in [15]. Then, the MDPC-SVM with power compensation (MDPC-SVM-PC) is examined to confirm the effectiveness of the power compensation derived in Section III-B. To decouple the influence of the dc voltage regulation on the control performance, the outer PI dc voltage controller is disabled in simulation tests and the rectifier works in power control mode. In the following tests, the original power references are set as $P^{\rm ref} = 1$ kW and $Q^{\rm ref} = 0$ var.

Fig. 4 shows the waveform of grid voltages U_{abc}, grid-side active power $P_{\rm in}$, grid-side reactive power $Q_{\rm in}$, and grid currents I_{abc} when there is 50% voltage dip in phase A. It is clear that $P_{\rm in}$ and $Q_{\rm in}$ can be regulated to follow their references accurately in the proposed MDPC-SVM. However, in the CDPC-SVM, there are obvious tracking errors with twice grid-frequency oscillations in the actual power. This test confirms that the conventional DPC-SVM cannot accurately force the actual power to track their references when grid voltages are unbalanced, whereas the proposed MDPC-SVM can work properly under an unbalanced network. As a power compensation strategy, as shown in

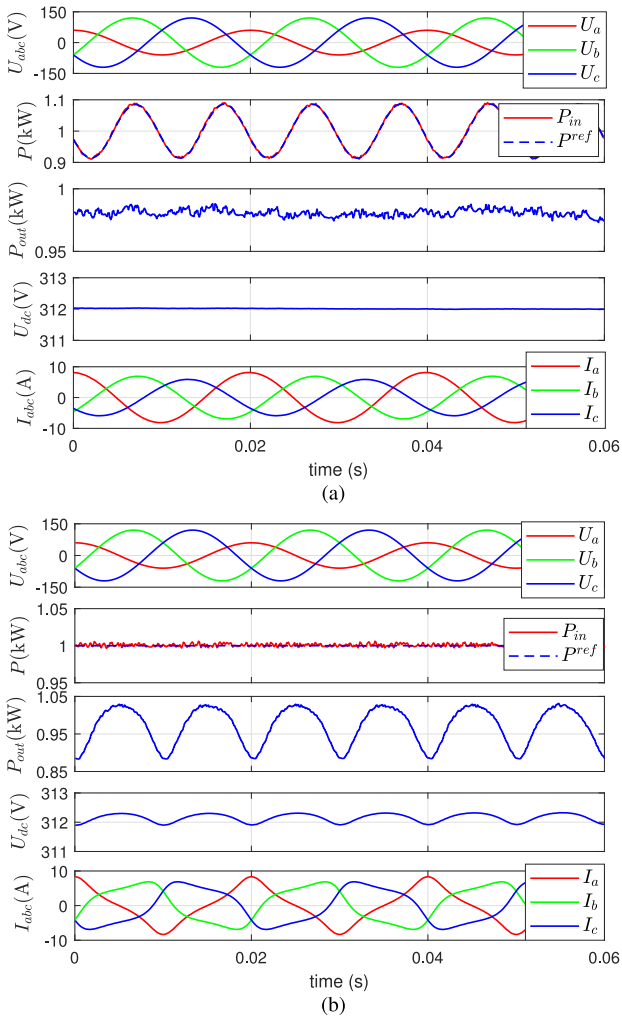

Fig. 5. Simulation results of U_{abc}, $P_{\rm in}$, $P^{\rm ref}$, $P_{\rm out}$, $U_{\rm dc}$, and I_{abc} for (a) MDPC-SVM-PC and (b) MDPC-SVM.

Section III-B, is not implemented, significant distortions can be seen in grid currents for both methods.

Fig. 5 shows simulation results of the proposed MDPC-SVM and MDPC-SVM-PC when there is 50% voltage dip in phase A. It can be seen that though grid-side power $P_{\rm in}$ presents oscillations, the converter-side power $P_{\rm out}$ and dc-link voltage $U_{\rm dc}$ are almost constant in MDPC-SVM-PC. On the contrary, $P_{\rm in}$ is constant in the MDPC-SVM. This results in oscillations in $P_{\rm out}$ and $U_{\rm dc}$. Additionally, grid currents are highly distorted in the MDPC-SVM, whereas i_{abc} are sinusoidal for the MDPC-SVM-PC. As MDPC-SVM-PC is the combination of MDPC-SVM and power compensation, as shown in (25) and (26), the superior performance of MDPC-SVM-PC over MDPC-SVM in this test validates the necessity of power compensation when grid voltages are unbalanced.

Fig. 6 shows simulation results when grid voltages change from a balanced condition to an unbalanced condition. At 0.05 s, 50% voltage dip in phase A is suddenly applied to evaluate the transient performance of MDPC-SVM-PC. It can be found that there is a drop in actual active power $P_{\rm in}$ after a sudden voltage sag. However, it can return to its reference quickly. With

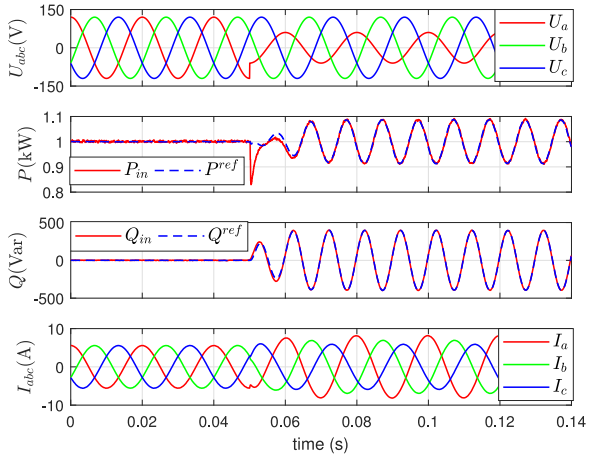

Fig. 6. Simulation results of MDPC-SVM-PC when 50% voltage dip in phase A is suddenly applied.

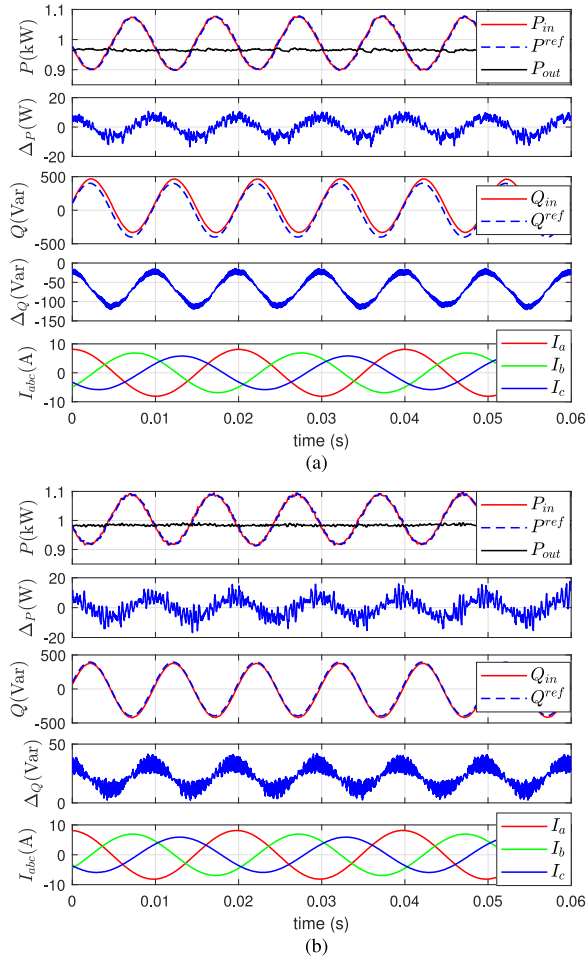

Fig. 7. Simulation results of MDPC-SVM-PC when both R and L in the controller are (a) 50% and (b) 150% of their actual value.

an ideal grid, both power references $P^{\rm ref}$ and $Q^{\rm ref}$ are kept the same as the original value. Hence, the proposed power compensation would not affect the normal operation when grid voltages are balanced. However, once the grid voltages are unbalanced, twice grid-frequency oscillations are added to original power

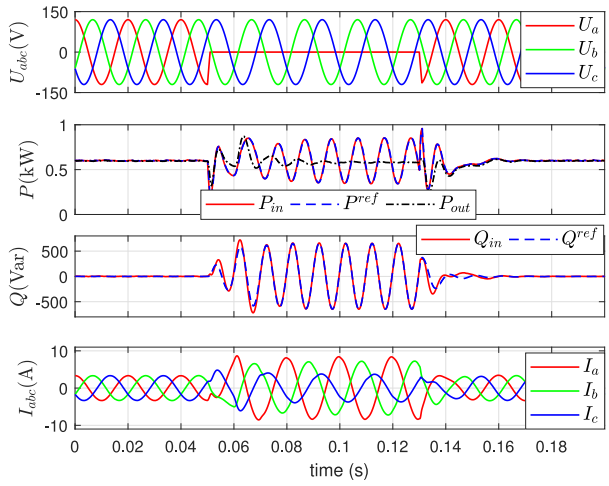

Fig. 8. Simulated results of MDPC-SVM-PC under one phase grounding fault.

references. As verified in Fig. 5, this helps to obtain a constant dc-link voltage and sinusoidal grid currents.

From simulation tests in this section, it can be concluded that the proposed MDPC-SVM-PC can accurately control the actual power under unbalanced grid conditions where the conventional DPC-SVM fails to work properly. Additionally, twice grid-frequency oscillations in the converter-side active power $P_{\rm out}$ and dc-link voltage $U_{\rm dc}$ can be removed while maintaining sinusoidal grid currents by the proposed power compensation.

To evaluate the robustness against parameter mismatches, the proposed MDPC-SVM-PC is tested when the inductance and resistance used in the controller are 50% and 150% of their actual values. The results are shown in Fig. 7. In the figure, $\Delta P = P^{\rm ref} - P_{\rm in}$ and $\Delta Q = Q^{\rm ref} - Q_{\rm in}$ are tracking errors of active power and reactive power, respectively. It is seen that there are some tracking errors in both active power and reactive power under parameter mismatches. However, the controller is still stable and works well under unbalanced grid conditions. Three-phase grid currents are sinusoidal and there is no oscillation in converter-side power $P_{\rm out}$. To eliminate the negative influence of parameter mismatches, it is suggested to use the online parameter identification technique, as shown in [11]. However, this part is out of scope of this paper and will not be further expanded.

Fig. 8 shows the simulated results of MDPC-SVM-PC when phase A is short circuited to the ground. It can be seen that when phase A voltage decreases to zero, the active power $P_{\rm in}$ can return to its reference quickly after a drop. With the proposed power compensation, the converter-side active power $P_{\rm out}$ can be kept constant without oscillations after transient process even under severely unbalanced grid conditions. Due to the voltage sag, the peak value of phase current is increased to maintain the output power. In practical application, power references may be limited as studied in [3] and [30] to avoid overcurrent when voltage sag occurs. After clearing of the fault, the system quickly recovers to the normal operation. This test further confirms that the proposed method can properly work under both ideal and unbalanced grid conditions.

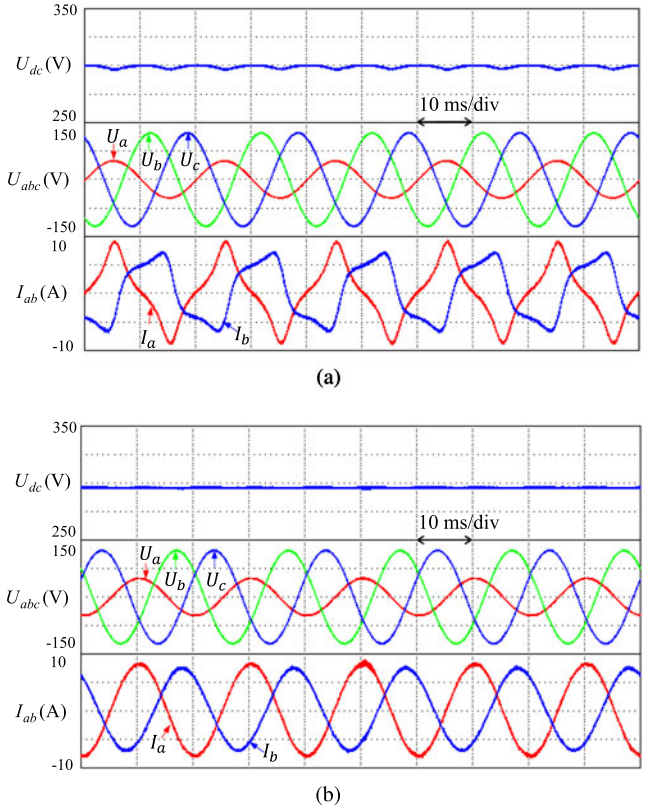

Fig. 9. Experimental results of (a) MDPC-SVM and (b) MDPC-SVM-PC under unbalanced grid conditions.

B. Experimental Results

To further confirm the effectiveness of the MDPC-SVM-PC, experimental results obtained from a two-level PWM rectifier under both balanced and unbalanced grid voltage conditions are presented. The results of MDPC-SVM without power compensation are also illustrated for comparison. A 32-b floating DSP TMS320F28335 was used to implement the control algorithm. The control and system parameters are the same as that used in the simulation, as listed in Table I. The block diagram of the proposed MDPC-SVM-PC is shown in Fig. 2. During experimental tests, unbalanced grid voltages are generated using a three-phase programmable ac source (Chroma 61511), in which 60% voltage dip in phase A is applied. The internal variables such as $P^{\rm ref}$, $P_{\rm in}$, $P_{\rm out}$, and $Q_{\rm in}$ are displayed on a digital oscilloscope via an on-board DA converter (DAC7724U), whereas the dc-link voltage $U_{\rm dc}$, three-phase grid voltages U_{abc}, and line currents I_{ab} are displayed on a ScopeCorder DL850, which are obtained directly by voltage and current probes. Similar to simulation tests, to clearly show the influence of power control on $U_{\rm dc}$ with unbalanced grid voltages, the dc voltage controller is disabled at the beginning of several tests. The obtained results are illustrated in Figs. 9–15. After that, outer PI controller is enabled to further verify the effectiveness of the proposed method in the closed-loop dc voltage regulation.

Fig. 9 shows comparative results for MDPC-SVM-PC and MDPC-SVM. It is seen that grid currents are significantly distorted in MDPC-SVM. Additionally, $U_{\rm dc}$ exists twice

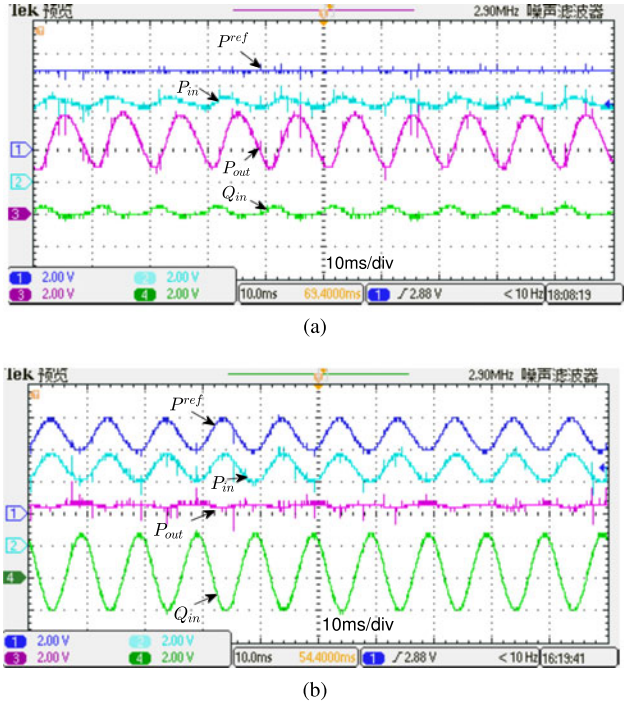

Fig. 10. Steady-state responses of P^{ref} (400 W/div), P_{in} (400 W/div), P_{out} (400 W/div), and Q_{in} [(a) 120 var/div, (b) 400 var/div] under unbalanced grid voltages for (a) MDPC-SVM, and (b) MDPC-SVM-PC.

grid-frequency oscillations. The peak-to-peak ripple of U_{dc} is about 1.67 V. If the proposed power compensation is implemented, the ripple in U_{dc} disappears, as can be seen in the responses of MDPC-SVM-PC. Although grid currents are unbalanced, they are sinusoidal in the shape for MDPC-SVM-PC. The experimental results are very similar to that presented in simulation. This test justifies again that the proposed power compensation can eliminate ripples in dc-link voltage while obtaining sinusoidal grid currents when grid voltage are unbalanced. From the corresponding responses of the active power and reactive power shown in Fig. 10, one can see that P_{in} in MDPC-SVM is kept constant. However, the converter-side active power P_{out} exists significant twice grid-frequency oscillations, which accounts for ripples in the dc-link voltage. With power compensation, though the grid-side power P_{in} is not a constant, the output power P_{out} presents much lower oscillations in MDPC-SVM-PC. This is conductive to obtain a dc-link voltage free from twice grid-frequency harmonics.

Fig. 11 shows the harmonic spectrum of one-phase grid current with power references as $P^{\mathrm{ref}} = 1000$ W and $Q^{\mathrm{ref}} = 0$ var for MDPC-SVM and MDPC-SVM-PC. To calculate harmonic components, the sampled current is transferred to the PC and analyzed by MATLAB function "fft." It can be clearly seen that the grid current contains significant harmonics in MDPC-SVM and the current THD is as high as 26.7%. On the contrary, by using the proposed power compensation, the current THD is only 1.43% in MDPC-SVM-PC, which is much lower than that of MDPC-SVM.

The dynamic responses of U_{dc} and i_{ab} are recorded in Fig. 12. In this test, the active power reference steps from 600 to 1000 W

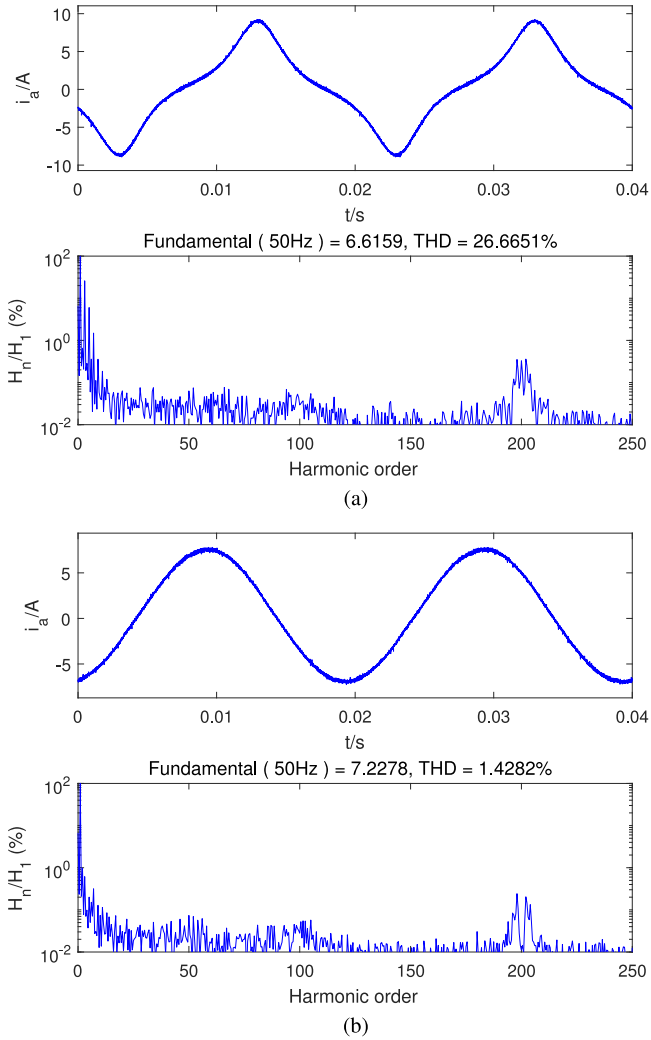

Fig. 11. Spectrum analysis of grid current for (a) MDPC-SVM and (b) MDPC-SVM-PC.

while Q^{ref} is kept at zero. It is seen that even during the transient process, grid currents are sinusoidal and there is no oscillations in U_{dc} for MDPC-SVM-PC. On the contrary, MDPC-SVM presents obvious ripples in U_{dc} and significant harmonics in grid currents. The corresponding power responses are shown in Fig. 13. For both methods, P_{in} can track P^{ref} quickly during the transient process. In MDPC-SVM, the original power reference is not modified, which is constant during the steady state. The output power P_{out} presents large twice grid-frequency harmonics. In MDPC-SVM-PC, both P^{ref} and Q^{ref} oscillate at twice grid frequency after employing power compensation. However, P_{out} is nearly constant during the steady-state operation. Hence, the ripple in U_{dc} is greatly reduced compared with that in MDPC-SVM.

From the above-mentioned tests, it can be concluded that MDPC-SVM-PC works well under unbalanced grid conditions, which can achieve constant dc-link voltage and sinusoidal grid currents when grid voltages are unbalanced. Its performance under an ideal grid condition is also tested and the result is shown in Fig. 14. It is seen that MDPC-SVM-PC works well with an

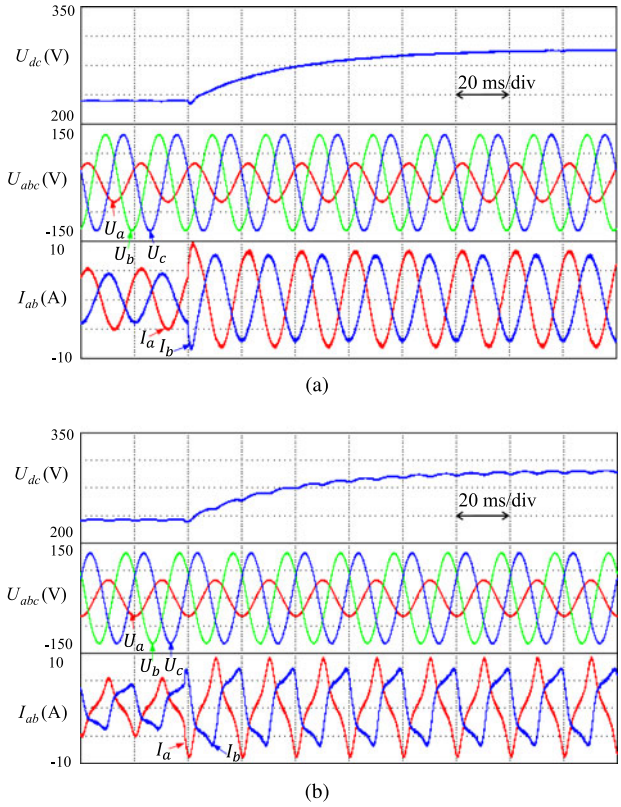

Fig. 12. Dynamic responses when P^{ref} steps from 600 W to 1 kW for (a) MDPC-SVM-PC and (b) MDPC-SVM under unbalanced grid conditions.

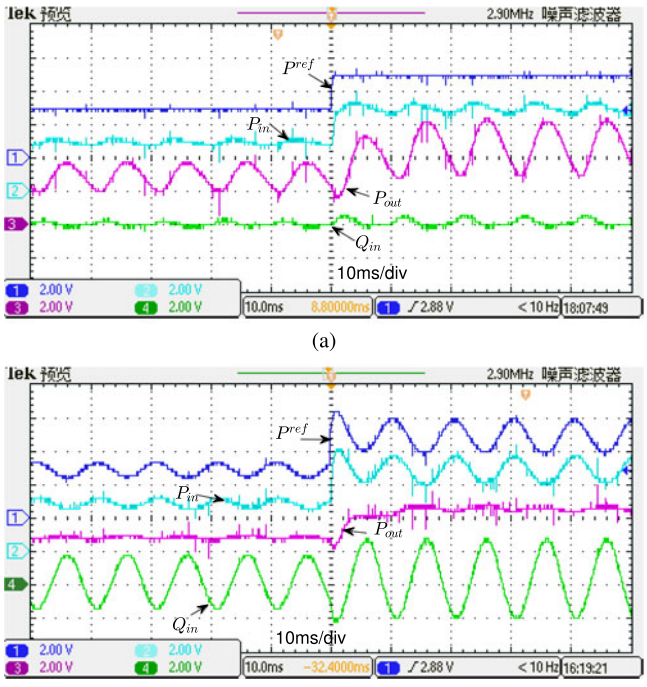

Fig. 13. Dynamic responses of P^{ref}(400 W/div), P_{in}(400 W/div), P_{out}(400 W/div), and Q_{in} [(a) 120 var/div, (b) 400 var/div] under unbalanced grid voltages when P^{ref} steps from 600 to 1000 W for (a) MDPC-SVM and (b) MDPC-SVM-PC.

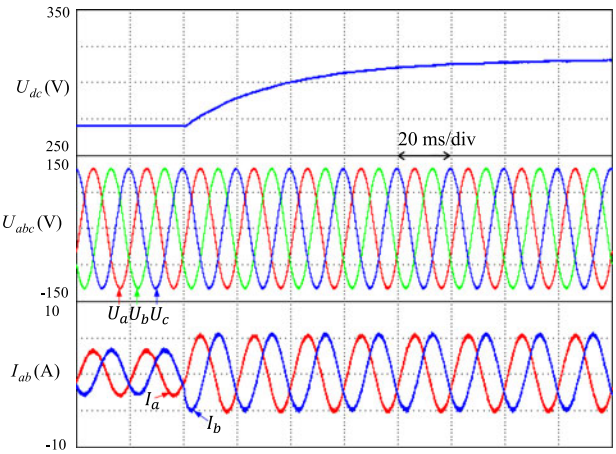

Fig. 14. Dynamic responses when P^{ref} steps from 600 W to 1 kW under ideal grid conditions for MDPC-SVM-PC.

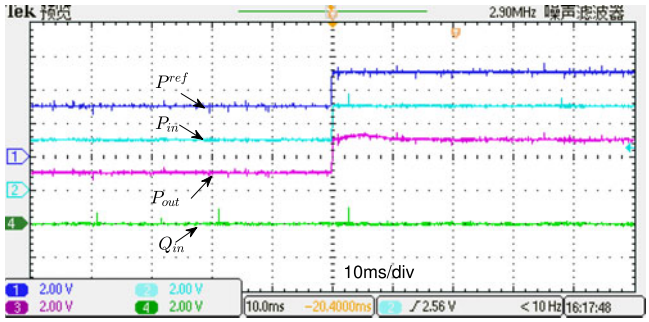

Fig. 15. Dynamic responses of MDPC-SVM-PC under ideal grid conditions when P^{ref} steps from 600 W to 1 kW. P^{ref}(400 W/div), P_{in}(400 W/div), P_{out}(400 W/div), and Q_{in}(400 var/div).

ideal grid. The current are sinusoidal and there are no ripples in dc-link voltage. From the power responses, as shown in Fig. 15, it can be found that power reference P^{ref} is a constant as same as the original power reference. There are no oscillations in active power P_{in}, P_{out}, and reactive power Q_{in} during the steady state. Hence, the proposed power compensation has no impact on the operation for an ideal grid, indicating that the proposed methods are applicable for both ideal and unbalanced grid conditions, as also confirmed in simulation results in Fig. 6.

After verifying the effectiveness of the proposed method on eliminating dc voltage oscillations in power control mode, the closed-loop dc voltage control is tested under unbalanced grid conditions. Fig. 16 shows responses of dc-link voltage when the external load is suddenly applied. In this test, $U_{\mathrm{dc}}^{\mathrm{ref}}$ is set as 300 V and the active power reference P^{ref} is generated by a PI controller, as shown in Fig. 2. It is seen that U_{dc} quickly returns to its reference after load is applied for both control schemes. However, MDPC-SVM suffers from significant dc voltage oscillations and distorted grid currents, whereas the proposed method presents much better performance in terms of smoother dc voltage and sinusoidal grid currents. This test further validates that the proposed method can effectively eliminate dc voltage oscillations under an unbalanced network.

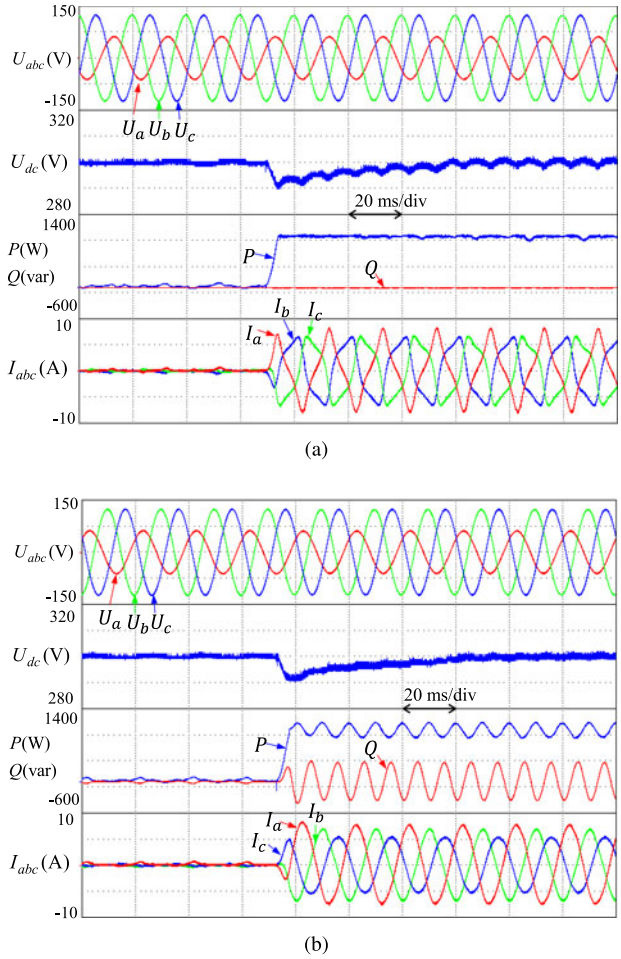

Fig. 16. Performance of the closed-loop dc-link voltage control when the external load is suddenly applied under unbalanced grid conditions for (a) MDPC-SVM and (b) MDPC-SVM-PC.

V. Conclusion

In the existing literature, most studies on DPC-SVM were carried out under balanced grid voltage conditions. Under unbalanced grid voltage conditions, the steady-state performance of DPC-SVM are seriously deteriorated by exhibiting highly distorted current and oscillations in the dc-link voltage. To cope with these problems, this paper proposed a novel DPC-SVM method, which is able to work effectively under both balanced and unbalanced grid conditions. An appropriate power compensation is derived, which only requires the grid/converter voltages and their delayed values. By adding this power compensation to the original power references without modifying the internal control structure, constant dc-link voltage and sinusoidal grid currents are achieved simultaneously without affecting the average value of grid-side active power and reactive power. The proposed DPC-SVM is compared to the conventional DPC-SVM and its effectiveness is confirmed by the presented simulation and experimental results.

Due to the additional calculation of power compensation, the complexity of the proposed DPC-SVM is higher than the conventional power control schemes. However, twice grid voltage frequency oscillations can be completely eliminated in theory by the proposed method under unbalanced grid conditions, which is beneficial to the lifetime and maintenance of capacitors. Though using a larger capacitor can also reduce dc voltage ripples, it may increase hardware cost and volume of the system. In this sense, the proposed method is more suitable for the application where a high-quality dc voltage is required under unbalanced grid conditions.

References

[1] Z. Zhang, H. Fang, F. Gao, J. Rodríguez, and R. Kennel, "Multiple-vector model predictive power control for grid-tied wind turbine system with enhanced steady-state control performance," *IEEE Trans. Ind. Electron.*, vol. 64, no. 8, pp. 6287–6298, Aug. 2017, doi: 10.1109/TIE.2017.2682000.

[2] A. Koran, T. LaBella, and J. S. Lai, "High efficiency photovoltaic source simulator with fast response time for solar power conditioning systems evaluation," *IEEE Trans. Power Electron.*, vol. 29, no. 3, pp. 1285–1297, Mar. 2014, doi: 10.1109/TPEL.2013.2262297.

[3] A. Camacho, M. Castilla, J. Miret, A. Borrell, and L. G. de Vicuña, "Active and reactive power strategies with peak current limitation for distributed generation inverters during unbalanced grid faults," *IEEE Trans. Ind. Electron.*, vol. 62, no. 3, pp. 1515–1525, Mar. 2015, doi: 10.1109/TIE.2014.2347266.

[4] W. Jiang, Y. Wang, J. Wang, L. Wang, and H. Huang, "Maximizing instantaneous active power capability for PWM rectifier under unbalanced grid voltage dips considering the limitation of phase current," *IEEE Trans. Ind. Electron.*, vol. 63, no. 10, pp. 5998–6009, Oct. 2016, doi: 10.1109/TIE.2016.2577544.

[5] H. Yang, Y. Zhang, J. Liang, J. Gao, P. Walker, and N. Zhang, "Sliding-mode observer based voltage-sensorless model predictive power control of PWM rectifier under unbalanced grid condition," *IEEE Trans. Ind. Electron.*, vol. 65, no. 7, pp. 5550–5560, Jul. 2018, doi: 10.1109/TIE.2017.2774730.

[6] V. Blasko and V. Kaura, "A new mathematical model and control of a three-phase ac-dc voltage source converter," *IEEE Trans. Power Electron.*, vol. 12, no. 1, pp. 116–123, Jan. 1997, doi: 10.1109/63.554176.

[7] J.-S. Yim, S.-K. Sul, B.-H. Bae, N. Patel, and S. Hiti, "Modified current control schemes for high-performance permanent-magnet ac drives with low sampling to operating frequency ratio," *IEEE Trans. Ind. Appl.*, vol. 45, no. 2, pp. 763–771, Mar./Apr. 2009, doi: 10.1109/TIA.2009.2013600.

[8] A. G. Yepes, A. Vidal, J. Malvar, O. Lòpez, and J. Doval-Gandoy, "Tuning method aimed at optimized settling time and overshoot for synchronous proportional-integral current control in electric machines," *IEEE Trans. Power Electron.*, vol. 29, no. 6, pp. 3041–3054, Jun. 2014, doi: 10.1109/TPEL.2013.2276059.

[9] Y. Zhang and C. Qu, "Table-based direct power control for three-phase ac/dc converters under unbalanced grid voltages," *IEEE Trans. Power Electron.*, vol. 30, no. 12, pp. 7090–7099, Dec. 2015, doi: 10.1109/TPEL.2014.2387694.

[10] J. Ge, Z. Zhao, L. Yuan, T. Lu, and F. He, "Direct power control based on natural switching surface for three-phase PWM rectifiers," *IEEE Trans. Power Electron.*, vol. 30, no. 6, pp. 2918–2922, Jun. 2015, doi: 10.1109/TPEL.2014.2377048.

[11] S. Kwak, U. C. Moon, and J. C. Park, "Predictive-control-based direct power control with an adaptive parameter identification technique for improved AFE performance," *IEEE Trans. Power Electron.*, vol. 29, no. 11, pp. 6178–6187, Nov. 2014, doi: 10.1109/TPEL.2014.2298041.

[12] Y. Zhang, C. Qu, and J. Gao, "Performance improvement of direct power control of PWM rectifier under unbalanced network," *IEEE Trans. Power Electron.*, vol. 32, no. 3, pp. 2319–2328, Mar. 2017, doi: 10.1109/TPEL.2016.2562262.

[13] A. Bouafia, J. P. Gaubert, and F. Krim, "Predictive direct power control of three-phase pulsewidth modulation (PWM) rectifier using space-vector modulation (SVM)," *IEEE Trans. Power Electron.*, vol. 25, no. 1, pp. 228–236, Jan. 2010, doi: 10.1109/TPEL.2009.2028731.

[14] Y. Zhang, Y. Bai, and H. Yang, "A universal multiple-vector-based model predictive control of induction motor drives," *IEEE Trans. Power Electron.*, 2017, doi: 10.1109/TPEL.2017.2754324.

[15] Y. Zhang and C. Qu, "Direct power control of a pulse width modulation rectifier using space vector modulation under unbalanced grid voltages," *IEEE Trans. Power Electron.*, vol. 30, no. 10, pp. 5892–5901, Oct. 2015, doi: 10.1109/TPEL.2014.2371469.

[16] Y. Zhang, Y. Peng, and H. Yang, "Performance improvement of two-vectors-based model predictive control of PWM rectifier," *IEEE Trans. Power Electron.*, vol. 31, no. 8, pp. 6016–6030, Aug. 2016, doi: 10.1109/TPEL.2015.2498306.

[17] Z. Li, Y. Li, P. Wang, H. Zhu, C. Liu, and W. Xu, "Control of three-phase boost-type PWM rectifier in stationary frame under unbalanced input voltage," *IEEE Trans. Power Electron.*, vol. 25, no. 10, pp. 2521–2530, Oct. 2010, doi: 10.1109/TPEL.2010.2049030.

[18] A. Yazdani *et al.*, "Modeling guidelines and a benchmark for power system simulation studies of three-phase single-stage photovoltaic systems," *IEEE Trans. Power Del.*, vol. 26, no. 2, pp. 1247–1264, Apr. 2011, doi: 10.1109/TPWRD.2010.2084599.

[19] J. R. Fischer, S. A. González, I. Carugati, M. A. Herrán, M. G. Judewicz, and D. O. Carrica, "Robust predictive control of grid-tied converters based on direct power control," *IEEE Trans. Power Electron.*, vol. 29, no. 10, pp. 5634–5643, Oct. 2014, doi: 10.1109/TPEL.2013.2294919.

[20] M. Mirhosseini, J. Pou, B. Karanayil, and V. G. Agelidis, "Resonant versus conventional controllers in grid-connected photovoltaic power plants under unbalanced grid voltages," *IEEE Trans. Sustain. Energy*, vol. 7, no. 3, pp. 1124–1132, Jul. 2016, doi: 10.1109/TSTE.2016.2529679.

[21] J. A. Suul, A. Luna, P. Rodríguez, and T. Undeland, "Virtual-flux-based voltage-sensor-less power control for unbalanced grid conditions," *IEEE Trans. Power Electron.*, vol. 27, no. 9, pp. 4071–4087, Sep. 2012, doi: 10.1109/TPEL.2012.2190301.

[22] Y. Suh and T. A. Lipo, "Modeling and analysis of instantaneous active and reactive power for PWM ac/dc converter under generalized unbalanced network," *IEEE Trans. Power Del.*, vol. 21, no. 3, pp. 1530–1540, Jul. 2006, doi: 10.1109/TPWRD.2005.860274.

[23] J. Eloy-Garcia, S. Arnaltes, and J. Rodriguez-Amenedo, "Direct power control of voltage source inverters with unbalanced grid voltages," *IET Power Electron.*, vol. 1, no. 3, pp. 395–407, 2008, doi: 10.1049/iet-pel:20070042.

[24] L. Shang, D. Sun, and J. Hu, "Sliding-mode-based direct power control of grid-connected voltage-sourced inverters under unbalanced network conditions," *IET Power Electron.*, vol. 4, no. 5, pp. 570–579, 2011, doi: 10.1049/iet-pel.2010.0160.

[25] Y. Zhang, J. Gao, and C. Qu, "Relationship between two direct power control methods for PWM rectifiers under unbalanced network," *IEEE Trans. Power Electron.*, vol. 32, no. 5, pp. 4084–4094, May 2017, doi: 10.1109/TPEL.2016.2593723.

[26] H. Akagi, Y. Kanazawa, and A. Nabae, "Instantaneous reactive power compensators comprising switching devices without energy storage components," *IEEE Trans. Ind. Appl.*, vol. IA-20, no. 3, pp. 625–630, May 1984, doi: 10.1109/TIA.1984.4504460.

[27] H.-S. Song and K. Nam, "Dual current control scheme for PWM converter under unbalanced input voltage conditions," *IEEE Trans. Ind. Electron.*, vol. 46, no. 5, pp. 953–959, Oct. 1999, doi: 10.1109/41.793344.

[28] Y. Zhang and C. Qu, "Model predictive direct power control of PWM rectifiers under unbalanced network conditions," *IEEE Trans. Ind. Electron.*, vol. 62, no. 7, pp. 4011–4022, Jul. 2015, doi: 10.1109/TIE.2014.2387796.

[29] J. Svensson, M. Bongiorno, and A. Sannino, "Practical implementation of delayed signal cancellation method for phase-sequence separation," *IEEE Trans. Power Del.*, vol. 22, no. 1, pp. 18–26, Jan. 2007, doi: 10.1109/TPWRD.2006.881469.

[30] A. Milicua, G. Abad, and M. A. R. Vidal, "Online reference limitation method of shunt-connected converters to the grid to avoid exceeding voltage and current limits under unbalanced operation–Part I: Theory," *IEEE Trans. Energy Convers.*, vol. 30, no. 3, pp. 852–863, Sep. 2015, doi: 10.1109/TEC.2015.2395718.

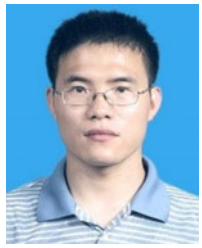

Yongchang Zhang (M'10–SM'18) received the B.S. degree from Chongqing University, Chongqing, China, in 2004, and the Ph.D. degree from Tsinghua University, Beijing, China, in 2009, both in electrical engineering.

From August 2009 to August 2011, he was a Postdoctoral Fellow with the University of Technology Sydney, Ultimo, NSW, Australia. In August 2011, he joined North China University of Technology as an Associate Professor. He is currently a Full Professor and the Director of Inverter Technologies Engineering Research Center of Beijing, North China University of Technology, Beijing. He has authored or coauthored more than 100 technical papers in the area of motor drives, pulsewidth modulation, and ac–dc converters. His current research focuses on model predictive control for power converters and motor drives.

Jie Liu was born in 1992. He received the B.S. degree in automation engineering in 2015 from North China University of Technology, Beijing, China, where he is currently working toward the M.S. degree in control science and engineering.

His current research focuses on control of pulsewidth modulation rectifiers.

Haitao Yang (S'16) received the B.S. degree from Hefei University of Technology, Hefei, China, in 2009, and the M.S. degree from North China University of Technology, Beijing, China, in 2015, both in electrical engineering. He is currently working toward the Ph.D. degree in mechanical engineering with the School of Mechanical and Mechatronic Engineering, University of Technology, Sydney, NSW, Australia.

His research interests include motor drives, position/speed sensorless control of ac motors, PWM converters, and electric vehicles.

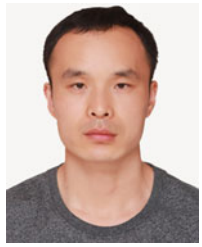

Jihao Gao was born in 1988. He received the B.S. degree from Henan University of Engineering, Zhengzhou, China, in 2013, and the M.S. degree from North China University of Technology, Beijing, China, in 2017, both in electrical engineering.

He is currently an Assistant Engineer with the Power Supply Department, Bejing Great Well Eletronic Equipment Co., Ltd., Beijing.